Multiloop Functional Renormalization Group That Sums Up All Parquet Diagrams

Fabian B. Kugler and Jan von Delft
Physics Department, Arnold Sommerfeld Center for Theoretical Physics, and Center for NanoScience, Ludwig-Maximilians-Universität München, Theresienstrasse 37, 80333 Munich, Germany

(Received 9 August 2017; published 31 January 2018)

We present a multiloop flow equation for the four-point vertex in the functional renormalization group (FRG) framework. The multiloop flow consists of successive one-loop calculations and sums up all parquet diagrams to arbitrary order. This provides substantial improvement of FRG computations for the four-point vertex and, consequently, the self-energy. Using the x-ray–edge singularity as an example, we show that solving the multiloop FRG flow is equivalent to solving the (first-order) parquet equations and illustrate this with numerical results.

DOI: 10.1103/PhysRevLett.120.057403

Introduction.—Two-particle correlations play a fundamental role in the theory of strongly correlated electron systems. Most response functions measured in condensed-matter experiments are two-particle quantities such as optical or magnetic susceptibilities. The behavior of the two-particle (or four-point) vertex has even been used to distinguish "weakly" and "strongly" correlated regions in the phase diagram of the Hubbard model [1]. Moreover, the four-point vertex is a crucial ingredient for a large number of theoretical methods to study strongly correlated electron systems, such as nonlocal extensions of the dynamical mean-field theory [2]—particularly, via dual fermions [3], the 1PI [4], and QUADRILEX [5] approach, or the dynamical vertex approximation [6]—the multiscale approach [7], the functional renormalization group [8,9], and the parquet formalism [10,11].

The parquet equations provide an exact set of self-consistent equations for vertex functions at the two-particle level and are thus able to treat particle and collective excitations on equal footing. In the first-order [10] (or so-called *parquet* [11]) approximation, they constitute a viable many-body tool [11–13] and, in logarithmically divergent perturbation theories, allow for an exact summation of all leading logarithmic diagrams of the four-point vertex (*parquet* diagrams [10]). It is a common belief [14] that results of the parquet approximation are equivalent to those of the one-loop renormalization group (RG). However, there is hardly any evidence of this statement going beyond the level of (static) flowing coupling constants [15].

Recently, the question was raised [16] whether it is possible to sum up all parquet diagrams using the functional renormalization group (FRG), a widely used realization of a quantum field-theoretical RG framework [8,9]. The parquet result for the x-ray–edge singularity (XES) [10,17–19] was indeed obtained [16], but using arguments that work only for this specific problem and do not apply generally [20]. In fact, the common truncation of the vertex-expanded FRG flow completely neglects contributions from the six-point vertex, which start at third order in the interaction. Schemes have been proposed for including some contributions from the six-point vertex [21–23]; however, until now it was not known how to do this in a way that captures all parquet diagrams.

In this work, we present a multiloop FRG (MFRG) scheme, which sums up all parquet diagrams to arbitrary order in the interaction. We apply it to the XES, a prototypical fermionic problem with a logarithmically divergent perturbation theory [24]; in a related publication [25], we develop the MFRG framework for general models. The XES allows us to focus on two-particle quantities, as these are solely responsible for the leading logarithmic divergence [10,17], and exhibits greatly simplified diagrammatics. In fact, it contains the minimal structure required to study the complicated interplay between different two-particle channels. We demonstrate how increasing the number of loops in the MFRG improves the numerical results with respect to the known solution of the parquet equations [10,17,18]. We establish the equivalence of the MFRG flow to the parquet approximation by showing that both schemes generate the same number of diagrams order for order in the interaction [26].

Model.—The minimal model for the XES is defined by the Hamiltonian

$$H = \sum_{\epsilon} \epsilon c_{\epsilon}^{\dagger} c_{\epsilon} + \epsilon_d d^{\dagger} d + U c^{\dagger} c d^{\dagger} d, \qquad U > 0. \tag{1}$$

Here, d and c_{ϵ}, respectively, annihilate an electron from a localized, deep core level ($\epsilon_d < 0$) or a half-filled conduction band with constant density of states ρ, half-bandwidth ξ_0, and chemical potential $\mu = 0$, while $c = \sum_{\epsilon} c_{\epsilon}$ annihilates a band electron at the core-level site. In order to describe optical properties of the system, one examines the particle-hole susceptibility $i\Pi(t) = \langle \mathcal{T} d^{\dagger}(t) c(t) c^{\dagger}(0) d(0) \rangle$. It exhibits a power-law divergence for frequencies close

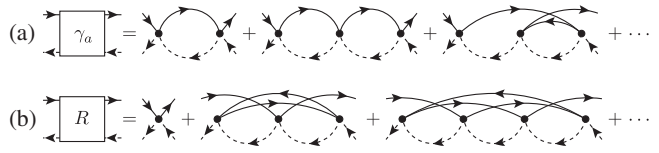

FIG. 1. Low-order diagrams for (a) the vertex reducible in antiparallel lines, γ_a, and (b) the totally irreducible vertex R. Solid (dashed) lines denote G^c (G^d), and a dot the bare vertex $-U$. The first-order or so-called parquet approximation only retains the bare vertex for R.

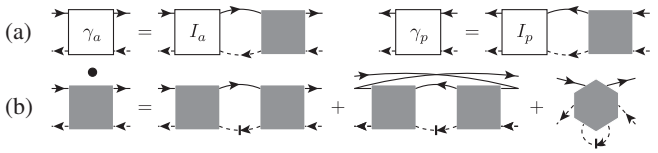

FIG. 2. (a) Bethe-Salpeter equations in the antiparallel (a) and parallel (p) channels. A full square denotes the full vertex $\Gamma^{(4)}$. (b) FRG flow equation for both channels relating $\partial_\Lambda \Gamma^{(4)}$ to $\Gamma^{(4)}$ and $\Gamma^{(6)}$. The conventional approximation is to set $\Gamma^{(6)} = 0$.

to the absorption threshold, as found both by the solution of parquet equations [10,17] and by an exact one-body approach [18].

In the Matsubara formalism, the bare level propagator reads $G^d_\omega = 1/(i\omega - \epsilon_d)$, and, focusing on infrared properties, we approximate the local band propagator as $G^c_\omega = -i\pi\rho \mathrm{sgn}(\omega)\Theta(\xi_0 - |\omega|)$. The particle-hole susceptibility takes the form (at a temperature $1/\beta \ll |\epsilon_d|$)

$$\Pi_{\bar{\omega}} = \frac{\rho}{\alpha(u)}\left[1 - \left(\frac{i\bar{\omega} + \epsilon_d}{-\xi_0}\right)^{-\alpha(u)}\right], \qquad u = \rho U, \quad (2)$$

where $\alpha(u) = 2u + O(u^2)$ and ϵ_d is considered as a renormalized threshold. The corresponding retarded correlation function is obtained by analytic continuation $i\bar{\omega} \to w + i0^+$, in which case the summands leading to the power law are logarithmically divergent as $u^n \ln^{n+1}(\xi_0/|w + \epsilon_d|)$. For imaginary frequencies, however, the perturbative parameter is finite, with a maximal value of $u \ln(\xi_0/|\epsilon_d|) \approx 0.9$, for our choice of parameters. Our goal will be to reproduce Eq. (2) using the FRG.

Parquet formalism.—The particle-hole susceptibility is fully determined by the one-particle-irreducible (1PI) four-point vertex via the following relation (using the shorthand notation $\Gamma^{(4)}_{\omega,\nu,\bar{\omega}} = \Gamma^{\bar{d}c\bar{c}d}_{\omega,\bar{\omega}+\omega,\bar{\omega}+\nu,\nu}$ [20]):

$$\Pi_{\bar{\omega}} = \frac{1}{\beta}\sum_\omega G^d_\omega G^c_{\bar{\omega}+\omega} + \frac{1}{\beta^2}\sum_{\omega,\nu} G^d_\omega G^c_{\bar{\omega}+\omega}\Gamma^{(4)}_{\omega,\nu,\bar{\omega}} G^d_\nu G^c_{\bar{\omega}+\nu}. \quad (3)$$

In principle, G^c and G^d are full propagators. However, for the XES, electronic self-energies do not contribute to the leading logarithmic divergence [10,17], and we can restrict ourselves to bare propagators.

Diagrams for the four-point vertex are exactly classified by the central parquet equation

$$\Gamma^{(4)} = R + \gamma_a + \gamma_p, \qquad I_a = R + \gamma_p, \qquad I_p = R + \gamma_a. \quad (4)$$

The leading divergence of the XES is determined by only two two-particle channels [10,17]: γ_a (cf. Fig. 1(a) [29]) and γ_p contain diagrams reducible by cutting two antiparallel or parallel lines, respectively, whereas I_a and I_p contain diagrams irreducible in the respective channel. The totally irreducible vertex R [cf. Fig. 1(b)] is the only input into the parquet equations, as the reducible vertices are determined self-consistently via Bethe-Salpeter equations [cf. Fig. 2(a)]. Similarly as for the self-energy, terms of R beyond the bare interaction only contribute subleadingly to the XES and can hence be neglected [10,17].

In this (parquet) approximation, Eq. (4) together with the Bethe-Salpeter equations for reducible vertices [Fig. 2(a)] form a closed set and can be solved. The analytic solution, employing logarithmic accuracy, provides the leading term of the exponent in Eq. (2). Our numerical solution, to which we compare all following results, is both consistent with the power-law-like behavior of Eq. (2) for small frequencies [cf. Fig. 4(c)] and with the corresponding exponent $\alpha(u)$ [cf. Fig. 4(d)].

Multiloop FRG flow.—The functional renormalization group provides an exact flow equation for the four-point vertex as a function of a RG scale parameter Λ, serving as infrared cutoff. Introducing Λ only in the bare d propagator, the flow encompassing both channels [26] is illustrated in Fig. 2(b), where the dashed arrow symbolizes the single-scale propagator S^d_Λ. Neglecting self-energies, we have $S^d_\Lambda = \partial_\Lambda G^d_\Lambda$, and $\partial_\Lambda \Gamma^{(4)}$ only depends on $\Gamma^{(4)}$ and $\Gamma^{(6)}$. The boundary conditions $G^d_{\Lambda_i} = 0$ and $G^d_{\Lambda_f} = G^d$ imply $\Gamma^{(4)}_{\Lambda_i} = -U$ and $\Gamma^{(6)}_{\Lambda_i} = 0$.

For almost all purposes, it is unfeasible to treat the six-point vertex exactly. Approximations of $\Gamma^{(6)}$ thus render the FRG flow approximate. The conventional approximation is to set $\Gamma^{(6)}$ and all higher-point vertices to zero, arguing that they are at least of third order in the interaction. This affects the resulting four-point vertex starting at third order and neglects terms that contribute to parquet diagrams [20]. Since, however, the parquet approximation involves *only* four-point vertices, it should be possible to encode the influence of six- and higher-point vertices during the RG flow by four-point contributions and, still, *fully* capture all parquet graphs.

In the following, we show how this can be accomplished using the MFRG. The first observation is that all the diagrammatic content of the truncated FRG (i.e., without $\Gamma^{(6)}$) is two-particle reducible, due to the bubble structure in the flow equation [first two summands of Fig. 2(b)], very similar to the Bethe-Salpeter equations [Fig. 2(a)]. The only irreducible contribution is the initial condition of the vertex, $\Gamma^{(4)}_{\Lambda_i} = -U$. Hence, diagrams generated by the flow are always of the parquet type. It is then natural to express $\Gamma^{(4)}$ as follows, using the channel classification of the parquet equations:

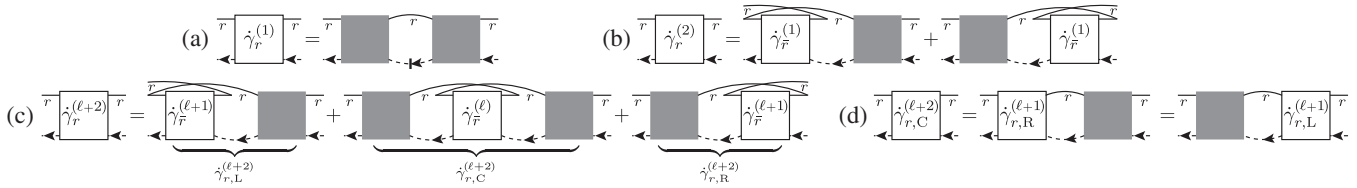

FIG. 3. Multiloop FRG flow equations, $\partial_\Lambda \gamma_r = \sum_{\ell \geq 1} \dot{\gamma}_r^{(\ell)}$, for the four-point vertex reducible in channel r, with $r = a$ or p, and $\bar{r} = p$ or a. The subscript r in the diagrams further symbolizes antiparallel or parallel c-d lines, respectively. (a) One-loop, (b) two-loop, (c) three- and higher-loop flows. (d) One-loop calculation of $\dot{\gamma}_{r,\mathrm{C}}^{(\ell+2)}$, using the previously computed $\dot{\gamma}_{r,\mathrm{R}}^{(\ell+1)}$ or $\dot{\gamma}_{r,\mathrm{L}}^{(\ell+1)}$.

$$\Gamma^{(4)} = -U + \gamma_a + \gamma_p, \qquad \partial_\Lambda \gamma_r = \sum_{\ell \geq 1} \dot{\gamma}_r^{(\ell)}. \tag{5}$$

Here, r stands for a or p and $\dot{\gamma}_r^{(\ell)}$ for diagrams involving ℓ loops connecting full vertices. We will show that $\dot{\gamma}_r^{(\ell)}$ can be constructed iteratively from lower-loop contributions.

The conventional (or *one-loop*) FRG flow in channel r is formulated in Fig. 3(a), where full vertices are connected by an r "single-scale" bubble, i.e., either antiparallel or parallel G^c-S^d lines. [Detailed diagrams with all arrows and their mathematical translations are given in Ref. [26], Fig. S2, Eq. (S2).] If one inserts the bare vertex for $\Gamma^{(4)}$ on the rhs of such a one-loop flow equation [Fig. 3(a)], one fully obtains the differentiated second-order vertex. However, inserting first- and second-order vertices on the rhs will miss some diagrams of the differentiated third-order vertex, because these invoke an $\bar{r}$ single-scale bubble that is not generated by $\dot{\gamma}_r^{(1)}$ (an overbar denotes the complementary channel: $\bar{a} = p$, $\bar{p} = a$). An example of such a missing third-order diagram is that obtained by differentiating the rightmost d propagator of the third diagram in Fig. 1(a) (cf. Fig. S1 of Ref. [26]). All such neglected contributions can be added to the rhs of the flow equation by hand (replacing bare by full vertices), resulting in the construction in Fig. 3(b). It uses an r "standard" bubble [(anti)parallel G^c-G^d lines] to connect the one-loop contribution from the complementary channel, $\dot{\gamma}_{\bar{r}}^{(1)}$, with the full vertex, thus generating *two*-loop contributions. These corrections have already been suggested from slightly different approaches [21,23].

The resulting third-order corrected flow will still miss derivatives of parquet graphs starting at fourth order in the interaction. These can be included via two further additions to the flow, which have the same form for all higher loop orders, $\dot{\gamma}_r^{(\ell+2)}$ with $\ell \geq 1$ [cf. Fig. 3(c)]. First, for the flow of $\dot{\gamma}_r^{(\ell+2)}$, an r bubble is used to attach the previously computed $(\ell+1)$-loop contribution from the complementary channel, $\dot{\gamma}_{\bar{r}}^{(\ell+1)}$, to either side of the full vertex, just as in the two-loop case. Second, by using two r bubbles, we include the differentiated ℓ-loop vertex from the complementary channel, $\dot{\gamma}_{\bar{r}}^{(\ell)}$, to the flow of $\dot{\gamma}_r^{(\ell+2)}$. Double counting of diagrams in all these contributions does not occur due to the unique position of the single-scale propagator [26]. Note that the central term in Fig. 3(c) can be computed by a one-loop integral, too, using the previous computations from the same channel, as shown in Fig. 3(d). Consequently, the numerical effort in the multiloop corrections scales linearly in ℓ.

By its diagrammatic construction, organized by the number of loops connecting full vertices, the MFRG flow incorporates *all* differentiated diagrams of a vertex reducible in channel r, built up from the bare interaction, and thus captures *all* parquet graphs of the full four-point vertex. Indeed, in Ref. [26], we prove algebraically for the XES that the number of differentiated diagrams in the MFRG matches precisely the number of differentiated parquet graphs. An ℓ-loop FRG flow generates *all* parquet diagrams up to order $n = \ell + 1$ in the interaction and, naturally, generates an increasing number of parquet contributions at arbitrarily large orders in U.

Numerical results.—In Fig. 5, we show numerical results for the XES particle-hole susceptibility. Using four different regulators (see below), we compare the susceptibility obtained from an ℓ-loop FRG flow to the numerical solution of the parquet equations. We find that the one-loop curves differ among each other and deviate strongly from the parquet result. With increasing loop order ℓ, the multiloop results from all regulators oscillate around and approach the parquet result, with very good agreement already for $\ell = 4$. For $\ell \geq 7$, the oscillations in the relative deviation (at $\bar{\omega} = 0$) are damped to $\lesssim 2\%$ (insets, solid line). A similar behavior is observed for the identity [30] $\Pi_{\bar{\omega}} = \lim_{|\omega|,|\nu| \to \infty} \gamma_{a;\omega,\nu,\bar{\omega}} / U^2$ ($\bar{\omega}$ is the exchange frequency, and ω, ν are two fermionic frequencies), which the parquet solution is guaranteed to fulfill (cf. Ref. [26], Eq. (S4) and following) (insets, dashed line).

As regulators, we choose the Litim regulator [31], and propagators of the type $G_\Lambda^d(\omega) = \theta(\omega/\Lambda - 1) G^d(\omega)$, where $\theta(x)$ is either a sharp, smooth, or oscillating step function (cf. Figs. 4(a) and 4(b); Eq. (S8) of Ref. [26]). The fact that different regulators give the same result in the MFRG flow is a strong indication for an exact resummation of diagrams.

Let us note that the MFRG flow also increases the stability of the solution towards larger interaction. Whereas, in the one-loop scheme, the four-point vertex diverges for $u > 0.4$, higher-loop schemes converge up to larger values of u. The reason is that the one-loop scheme contains the *full* ladder series of diagrams (in any channel), but only

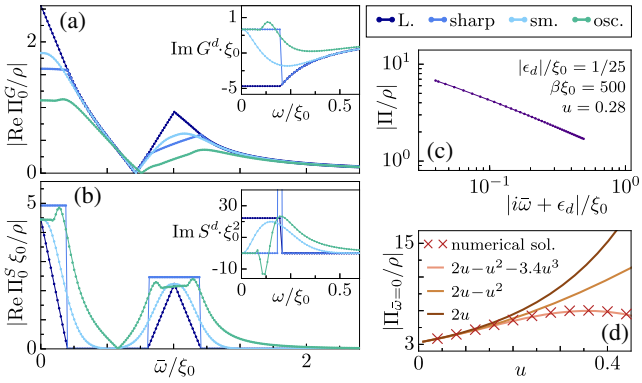

FIG. 4. (a) Noninteracting "standard" particle-hole bubble Π_0^G and propagator G^d (inset) for different regulators (cf. Eq. (S8) of Ref. [26]) and $\Lambda/\xi_0 = 0.2$. (b) Same as (a) for the "single-scale" bubble Π_0^S and propagator S^d. (c) Double-logarithmic plot for the particle-hole susceptibility Π, obtained from solving the parquet equations. (d) $\Pi_{\bar\omega=0}(u)$ computed via the parquet equations [ϵ_d, β as in (c)] and according to Eq. (2) with different choices for $\alpha(u)$. The comparison between these guide-to-the-eye lines and the numerical solution confirms that $\alpha(u) \approx 2u$, but also shows that subleading contributions become sizable for larger u. These are present since internal numerical calculations go beyond logarithmic accuracy.

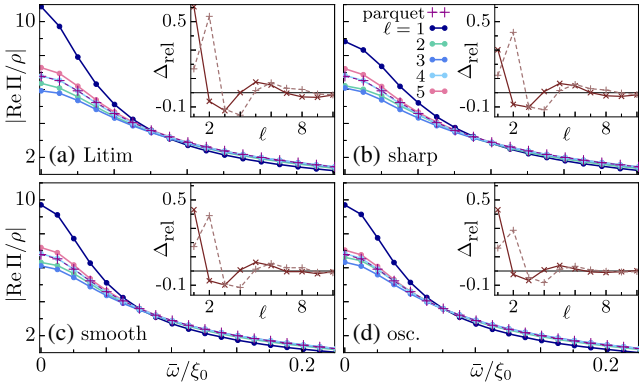

FIG. 5. (a)–(d) Numerical solutions for the particle-hole susceptibility Π, obtained from the parquet equations and from MFRG with different regulators [cf. Figs. 4(a) and 4(b)], using the parameters of Fig. 4(c). Insets: Relative deviation between parquet and MFRG results for Π (solid line) and between Π and $\lim_{|\omega|,|\nu|\to\infty}\gamma_a/U^2$ (dashed line), all evaluated at $\bar\omega = 0$.

parts of nonladder diagrams. Whereas the (imaginary-frequency) pure particle-hole ladder already diverges at $u \sim 0.3$, higher-loop extensions approaching the parquet summation are needed for the full feedback between both channels to eliminate the divergence.

The equivalence between the MFRG flow and parquet summation allows us to explain how the quality of FRG results depends on the choice of regulator. Whereas the one-loop scheme only involves a single-scale bubble $\Pi_0^S = \sum G^c S^d$, all extensions invoke successive standard bubbles $\Pi_0^G = \sum G^c G^d$. By minimizing the weight of Π_0^G compared to Π_0^S, one minimizes the effect of the multiloop corrections and thus the difference between low-level MFRG and parquet. Indeed, from Figs. 4(a) and 4(b) we see that a regulator with small (large) weight in Π_0^G and large (small) weight in Π_0^S, such as the oscillating-step (Litim) regulator, gives comparatively good (bad) agreement with parquet for low ℓ. Accordingly, the sharp-step regulator performs slightly better than its smooth counterpart.

Generalizations.—The MFRG flow can be readily extended to more general models, where one normally does not treat two particle species separately, as done here for c and d electrons. If three two-particle channels (antiparallel, parallel, and transverse) are involved, the higher-loop flow must incorporate feedback from both complementary channels via $\dot\gamma_r^\ell = \sum_{r'\neq r}\dot\gamma_{r'}^\ell$ [25]. The self-energy Σ enters the $\Gamma^{(4)}$ flow via full propagators, and, in the one-loop flow of the four-point vertex [Fig. 3(a)], one should follow the usual practice [8,21] of using the derivative of the full propagator ($\partial_\Lambda G_\Lambda$) instead of the single-scale propagator ($S_\Lambda = \partial_\Lambda G_\Lambda|_{\Sigma=\mathrm{const}}$) which excludes any differentiated self-energy contributions. The reason is that, in the exact FRG flow equation [Fig. 2(b)], those diagrams of $\partial_\Lambda\Gamma^{(4)}$ that involve $\partial_\Lambda\Sigma$ are encoded in the six-point vertex.

Evidently, an improved flow for $\Gamma^{(4)}$ also improves FRG calculations of the self-energy. In the parquet formalism, Σ is constructed from the four-point vertex by an exact, self-consistent Schwinger-Dyson equation [11]. In order to obtain the same self-energy diagrams from the (in principle) *exact* FRG flow equation for Σ, with only the vertex in the parquet *approximation* at one's disposal, multiloop extensions to the self-energy flow, similar to those introduced here, can be performed [25]. Given the self-energy, all arguments about capturing parquet diagrams (which now consist of dressed lines) with the multiloop FRG flow remain valid since they only involve generic, model-independent statements about the structure of two-particle diagrams.

The MFRG flow is applicable for any initial condition $\Gamma^{(4)}_{\Lambda_i}$. An example where one would not start from $G_{\Lambda_i} = 0$, as done here, arises in the context of dynamical mean-field theory (DMFT) [2]. There, the goal of adding nonlocal correlations, with the local vertex from DMFT ($\Gamma^{(4)}_{\mathrm{DMFT}}$) as input, can be pursued using the FRG [32]. Alternatively, this goal is also being addressed by using the parquet equations in the dynamical vertex approximation (DΓA) [6]. However, the latter approach requires the *diagrammatic* decomposition of the *nonperturbative* vertex [33] $\Gamma^{(4)}_{\mathrm{DMFT}} = R + \sum_r \gamma_r$, which yields diverging results close to a quantum phase transition [1,35]. In contrast, the MFRG flow is built from the *full* vertex $\Gamma^{(4)}_{\mathrm{DMFT}}$ and could thus be used to scan a larger region of the phase diagram.

Conclusion.—Using the x-ray–edge singularity as an example, we have presented multiloop FRG flow equations, which sum up all parquet diagrams to arbitrary order,

so that solving the MFRG flow is equivalent to solving the (first-order) parquet equations. Our numerical results demonstrate that solutions of an ℓ-loop flow quickly approach the parquet result with increasing ℓ. This applies for a variety of regulators, confirming an exact resummation of diagrams. The MFRG construction is generic and can be readily generalized to more complex models.

The MFRG-parquet equivalence established here shows that one-loop FRG calculations generate only a subset of (differentiated) parquet diagrams and that a multiloop FRG flow is needed to reproduce parquet results. From a practical point of view, the MFRG appears advantageous over solving the parquet equations since solving a first-order ordinary differential equation is numerically more stable than solving a self-consistent equation. Moreover, one can choose a suitable regulator and flow from any initial action. Altogether, the MFRG scheme achieves, in effect, a solution of the (first-order) parquet equations while retaining all treasured FRG advantages: no need to solve self-consistent equations, purely one-loop costs, and freedom of choice for regulators.

We thank A. Eberlein, C. Honerkamp, S. Jakobs, V. Meden, W. Metzner, and A. Toschi for useful discussions and acknowledge support by the Cluster of Excellence Nanosystems Initiative Munich. F. B. K. acknowledges funding from the research school IMPRS-QST.

[1] T. Schäfer, G. Rohringer, O. Gunnarsson, S. Ciuchi, G. Sangiovanni, and A. Toschi, Phys. Rev. Lett. **110**, 246405 (2013).
[2] A. Georges, G. Kotliar, W. Krauth, and M. J. Rozenberg, Rev. Mod. Phys. **68**, 13 (1996).
[3] A. N. Rubtsov, M. I. Katsnelson, and A. I. Lichtenstein, Phys. Rev. B **77**, 033101 (2008); S. Brener, H. Hafermann, A. N. Rubtsov, M. I. Katsnelson, and A. I. Lichtenstein, Phys. Rev. B **77**, 195105 (2008); H. Hafermann, G. Li, A. N. Rubtsov, M. I. Katsnelson, A. I. Lichtenstein, and H. Monien, Phys. Rev. Lett. **102**, 206401 (2009).
[4] G. Rohringer, A. Toschi, H. Hafermann, K. Held, V. I. Anisimov, and A. A. Katanin, Phys. Rev. B **88**, 115112 (2013).
[5] T. Ayral and O. Parcollet, Phys. Rev. B **94**, 075159 (2016).
[6] A. Toschi, A. A. Katanin, and K. Held, Phys. Rev. B **75**, 045118 (2007); K. Held, A. A. Katanin, and A. Toschi, Prog. Theor. Phys. Suppl. **176**, 117 (2008); A. Valli, G. Sangiovanni, O. Gunnarsson, A. Toschi, and K. Held, Phys. Rev. Lett. **104**, 246402 (2010).
[7] C. Slezak, M. Jarrell, T. Maier, and J. Deisz, J. Phys. Condens. Matter **21**, 435604 (2009).
[8] W. Metzner, M. Salmhofer, C. Honerkamp, V. Meden, and K. Schönhammer, Rev. Mod. Phys. **84**, 299 (2012).
[9] P. Kopietz, L. Bartosch, and F. Schütz, *Introduction to the Functional Renormalization Group*, Lecture Notes in Physics (Springer, Berlin, 2010).
[10] B. Roulet, J. Gavoret, and P. Nozières, Phys. Rev. **178**, 1072 (1969).
[11] N. Bickers, in *Theoretical Methods for Strongly Correlated Electrons*, edited by D. Sénéchal, A.-M. Tremblay, and C. Bourbonnais, CRM Series in Mathematical Physics (Springer, New York, 2004), pp. 237–296.
[12] A. Valli, T. Schäfer, P. Thunström, G. Rohringer, S. Andergassen, G. Sangiovanni, K. Held, and A. Toschi, Phys. Rev. B **91**, 115115 (2015).
[13] G. Li, N. Wentzell, P. Pudleiner, P. Thunström, and K. Held, Phys. Rev. B **93**, 165103 (2016).
[14] A. Gogolin, A. Nersesyan, and A. Tsvelik, *Bosonization and Strongly Correlated Systems* (Cambridge University Press, Cambridge, England, 2004), p. 332.
[15] D. Zanchi and H. J. Schulz, Phys. Rev. B **61**, 13609 (2000); R.-Q. Xing, L. Classen, M. Khodas, and A. V. Chubukov, Phys. Rev. B **95**, 085108 (2017); C. Bourbonnais, in *Strongly Interacting Fermions and High-Tc Superconductivity*, edited by B. Douçout and J. Zinn-Justin (Elsevier Sience, Amsterdam, 1995), pp. 307–369.
[16] P. Lange, C. Drukier, A. Sharma, and P. Kopietz, J. Phys. A **48**, 395001 (2015).
[17] P. Nozières, J. Gavoret, and B. Roulet, Phys. Rev. **178**, 1084 (1969).
[18] P. Nozières and C. T. De Dominicis, Phys. Rev. **178**, 1097 (1969).
[19] G. D. Mahan, Phys. Rev. **163**, 612 (1967).
[20] F. B. Kugler and J. von Delft, arXiv:1706.06872.
[21] A. A. Katanin, Phys. Rev. B **70**, 115109 (2004).
[22] M. Salmhofer, C. Honerkamp, W. Metzner, and O. Lauscher, Prog. Theor. Phys. **112**, 943 (2004).
[23] A. Eberlein, Phys. Rev. B **90**, 115125 (2014).
[24] T. Giamarchi, *Quantum Physics in One Dimension* (Clarendon Press, Oxford, 2004), p. 347.
[25] F. B. Kugler and J. von Delft, Phys. Rev. B **97**, 035162 (2018).
[26] See Supplemental Material at http://link.aps.org/supplemental/10.1103/PhysRevLett.120.057403 for the technical details used in our calculations, which includes Refs. [27,28].
[27] I. Gradshteyn and I. Ryzhik, *Table of Integrals, Series, and Products*, edited by A. Jeffrey and D. Zwillinger (Academic Press, Boston, 2007), 7th ed., p. 990.
[28] N. J. A. Sloane, The On-Line Encyclopedia of Integer Sequences (Mar. 2017), published electronically at https://oeis.org.
[29] Since, in a zero-temperature real-frequency treatment [10] of x-ray absorption, G^d is purely advanced, we draw diagrams such that all G^d lines are oriented to the left.
[30] N. Wentzell, G. Li, A. Tagliavini, C. Taranto, G. Rohringer, K. Held, A. Toschi, and S. Andergassen, arXiv:1610.06520.
[31] D. F. Litim, Phys. Rev. D **64**, 105007 (2001).
[32] C. Taranto, S. Andergassen, J. Bauer, K. Held, A. Katanin, W. Metzner, G. Rohringer, and A. Toschi, Phys. Rev. Lett. **112**, 196402 (2014).
[33] Alternatives to DΓA which do not require the totally irreducible vertex are the dual fermion [3] and the related 1PI approach [4]. However, upon transformation to the dual variables, the bare action contains n-particle vertices for all n. Recent studies [34] show that the corresponding six-point

vertex yields sizable contributions for the (physical) self-energy, and it remains unclear how a truncation in the (dual) bare action can be justified.

[34] T. Ribic, G. Rohringer, and K. Held, Phys. Rev. B **95**, 155130 (2017); T. Ribic, P. Gunacker, S. Iskakov, M. Wallerberger, G. Rohringer, A. N. Rubtsov, E. Gull, and K. Held, Phys. Rev. B **96**, 235127 (2017).

[35] T. Schäfer, S. Ciuchi, M. Wallerberger, P. Thunström, O. Gunnarsson, G. Sangiovanni, G. Rohringer, and A. Toschi, Phys. Rev. B **94**, 235108 (2016); O. Gunnarsson, G. Rohringer, T. Schäfer, G. Sangiovanni, and A. Toschi, Phys. Rev. Lett. **119**, 056402 (2017).